SAND99-2412J

PROCESSING, MICROSTRUCTURE AND ELECTRIC PROPERTIES OF BURIED RESISTORS IN LOW TEMPERATURE CO-FIRED CERAMICS

Pin Yang, Mark A. Rodriguez, Paul Kotula, Brandon K. Miera and Duane B. Dimos
Sandia National Laboratories, Albuquerque, NM 87185-0959

ABSTRACT

The electrical properties were investigated for ruthenium oxide based devitrifiable resistors embedded within low temperature co-fired ceramics. Special attention was given to the processing conditions and their affects on resistance and temperature coefficient of resistance (TCR). Results indicate that the conductance for these buried resistors is limited by tunneling of charge carriers through the thin glass layer between ruthenium oxide particles. A modified version of the tunneling barrier model is proposed to more accurately account for the microstructure ripening observed during thermal processing. The model parameters determined from curve fitting show that charging energy (i.e., the energy required for a charge carrier to tunnel through the glass barrier) is strongly dependent on particle size and particle-particle separation between ruthenium oxide grains. Initial coarsening of ruthenium oxide grains was found to reduce the charging energy and lower the resistance. However, when extended ripening occurs, the increase in particle-particle separation increases the charging energy, reduces the tunneling probability and gives rise to a higher resistance. The trade-off between these two effects results an optimum microstructure with a minimum resistance and TCR. Furthermore, the TCR of these resistors has been shown to be governed by the magnitude of the charging energy. Model parameters determined by our analysis appear to provide quantitative physical interpretations to the microstructural change in the resistor, which in turn, are controlled by the processing conditions.

DISCLAIMER

INTRODUCTION

(I) Buried Resistor

The oxide-based thick film resistors are ceramic-glass composites that are used extensively in hybrid microcircuits. The small temperature coefficient of resistance (TCR) of thick film resistors is attractive for systems that encounter a wide range of service temperatures or for use in a high power dissipation environment, such as automotive electronics and high-density electronic packages. With recent trends in component miniaturization, many passive components such as resistors, capacitors and inductors are being integrated into multi-layer structures. In this paper, we report the effects of processing conditions on the electrical properties of buried resistors. Special attention has been placed on microsturctural development and the associated changes in resistance and temperature coefficient of resistance (TCR) of these buried resistor components.

The resistor ink used in this investigation is an experimental ink from DuPont (E84005-140). This particular resistor ink has been specifically designed for fabrication of buried components using DuPont low temperature co-firable ceramic (LTCC) tapes (DuPont A951). The glass materials in the resistor and LTCC tape are adjusted to minimize the differential shrinkage during firing to prevent distortion of the fired parts. At high temperature the specially formulated, highly viscous glass, rapidly devitrifies from glass to ceramic (above 820 °C). The devitrification process serves to prevent glass infiltration from the dielectric layers and obviate any extended chemical reactions between resistors and dielectric tape. The devitrification process in the co-fired resistor ink is unique; in most conventional post-fire inks the glass remains in a glassy state after melting. In previous studies[1-2], significant devitrification of the glass phase has been observed for both the experimental resistor ink and LTCC tape. Detailed chemical reaction and microstructure development of buried resistors prepared between 835 and 875 °C for various holding times have been reported elsewhere.[2]

The thick film resistors are typically prepared by screen-printing of a suitable resistor paste onto a dielectric substrate. The resistor paste consists of a fine-grained ($\leq$10 nm) conductive oxide powder mixed with larger ($\approx$ 1μm), nonconductive glass particles and an organic medium that provides proper rheology for printing. The

resistance of these resistors can be adjusted by the volume fraction of conductive oxide in the paste.[3-4] The microstructure of printed resistors can be described as a random array of glass particles with conductive oxide residing in the interstices between the glass particles. The printed circuit pattern then undergoes a drying and a firing processes where the organic material is gradually burned out and, at a sufficiently high temperature, the glass melts and wets the oxide particles, thereby forming thin barrier layers between the conductive grains. Under a weak field, charge carriers will tunnel through these glass barriers[4] to provide a conducting path through the three-dimensional network of conductive particle chains. As a result, the electrical properties of these resistors are often strongly dependent on the final microstructure, which is in turn, correlated to the processing conditions. Therefore, precision control of the thermal process is essential to assure reproducibility as well as achieve high precision and tolerance of fabricated circuits. This is especially true for circuits fabricated with buried resistors where additional trimming of these components after firing is not a viable option.

(II) Tunneling Barrier Model

A tunneling-barrier model proposed by Pike and Seager[4] has successfully described the electrical conduction mechanisms in thick film resistors. According to the model, the temperature dependence of resistance R(T) of a thick film resistor under a low electrical field is determined by summing the resistance of the conductive particles and the resistance of the glass barrier separating the conducting particles. This can be expressed by the following equation:

$$R(T) = \frac{1}{2} R_{bo} \left(\frac{\sin aT}{aT} \right) \left[1 + \exp\left(\frac{E}{kT} \right) \right] + R_{mo}(1 + bT), \qquad (1)$$

where T is the absolute temperature, a is related to the tunneling probability, E is the electrostatic charging energy, k is Boltzmann's constant, R_{bo} is a lump term accounting for two different contributions to the overall tunneling mechanism, and R_{mo} is the metallic-phase resistance if the temperature were extrapolated to absolute zero.

The $\sin(aT)/aT$ term describes the weak temperature dependence of tunneling through insulating films, and a is the first coefficient of a Taylor expansion of the natural logarithm of the tunneling probability and can be estimated by the insulator barrier

height.[5] Typically, a increases as the tunneling probability decreases. The exponential term in Eq. (1) acounts for the equilibrium number of charge carriers with charge energy of E, based on the Fermi-Dirac distribution. E is described as the charging energy required to transfer one charge carrier from one particle to the next, strictly based on classical electrostatic behavior. Charge carriers with charge energy greater than E are capable of making the tunneling transition. The rightmost terms in Eq. (1) depict the temperature dependence of the resistance for metallic oxide particles.

Based on this model, the overall temperature effects give a rather flat R(T) curve with a shallow minimum, as shown in the example of Fig. 1.[6] This result is obtained from the electrical measurement of a traditional post-fired resistor (DuPont 1731). At temperatures below the resistance minimum temperature (T_m), the overall conductance is limited by the number of charge carriers that can tunnel through the glass barriers. As the temperature increases, the overall contribution from the tunneling effect gives a negative slope for R(T) because the number of charge carriers readily available for tunneling increases with temperature, according to Fermi-Dirac statistics. As temperature further increases, the limiting conduction mechanism in the resistor is progressively changing from a tunneling mechanism to that of a thermal scattering of charge carriers within the conductive oxide particles. Hence, the resistance can no longer continue to decrease, resulting in a resistance minimum on the R(T) curve. Above T_m, the overall conductance is limited by the thermal scattering of charge carriers and exhibits a positive, essentially linear, increase with temperature that is characteristic of metallic conduction.

Because each term in Eq. (1) represents a different physical factor contributing to the overall changes in resistance, analyzing the changes of these factors with respect to processing conditions can provide insights about the influence of process parameters on final properties and can also serve as a guideline for process control. In this investigation, the objective is to provide a physical interpretation of the changes in electrical properties with respect to the processing conditions. These interpretations are based on the model parameters determined from the curve fitting of R(T) measurements and the correlation of these measurements to the processing conditions and observed microstructures for these thick film resistors. In this study, we have slightly modified the original tunneling barrier model[4] to more accurately account for the changes in tunneling

probability due to Ostwald ripening of the conductive oxide grains during a prolonged thermal process. Details of this modification shall be presented later in the results and discussion section.

EXPERIMENTAL PROCEDURE

It is well known to the thick film hybrid microcircuit industry that precision control of print thickness and firing temperature are the key factors in assuring the reproducibility of resistors in a microcircuit. Since the objective of this investigation is to understand the changes in electrical properties with respect to different processing conditions, special attention was paid to minimize these variations so that contributions from these factors could be excluded.

Because a traditional screen-printing process produces a thinner layer at the center of a pattern than at the edges, a direct-write Micropen system was used to deposit the resistor pattern onto the low temperature co-fired green tape (DuPont A951). The Micropen system, equipped with a computer controlled feedback system, provides excellent control of print thickness and edge definition which in turn gives a tighter control over the printed width. Previous results have shown that the Micropen precisely controlled the printed thicknesses to with ±1.5 μm, and resistors fabricated by the Micropen held a tighter tolerance compared to those made by a conventional screen printing process.[7] The print thickness of the resistors in this study was set at 30 μm. This thickness was chosen because previous results indicated that resistors made of this print thickness were less sensitive to changes in resistance due to small thickness variations (see Figure 2, open circles).[7] A similar trend was observed for resistors post-fired on alumina substrates (solid circles with error bars). Since both the resistor and conductor (DuPont 6142D) inks are compatible with LTCC green tape (DuPont A951), the resistor pattern was deposited prior to the conductor traces to minimize the thickness variation of the resistor close to the conductor pattern. The resistor pattern was designed to give an aspect ratio of 1.2:1 (or 1.2 squares), with a width of 50 mils (0.127 cm). There were six layers of green tape used to build the test circuits. The printed pattern was deposited on the second layer from the top surface and electrical connections were made through

conductor filled via holes. Each pattern consisted of 20 resistors. The green tapes were cross-laminated under hydrostatic pressure (3000 psi) at 68 °C.

After lamination, the samples were fired in a box furnace. To assure the temperature uniformity, samples were placed in the middle of a rectangular quartz tube with two thermocouples placed on each side. Data obtained from a chart recorder indicated that the temperature difference between these thermocouples was less than 2 °C at the peak firing temperature. Samples were fired with a heating rate of 5 °C/min with a two hour soak at 450 °C to burn out the organic in the green structure. The peak firing temperatures were set at 825, 835, 850, and 875 °C for various holding times. After firing, samples were furnace cooled to room temperature.

The resistance values at room temperature were determined by a four-point measurement from a digital multimeter (HP 3457A). Data were reported as the average value of 20 resistors. The sheet resistance was determined by the resistance value divided by the number of squares in the resistor pattern (correcting for the ratio 1.2 for each square). R(T) curves were obtained by placing samples in a temperature controlled chamber equipped with an automatic data acquisition setup. Resistance values were collected from –100 °C to 100 °C at a heating rate of 3 °C/min. The slope of resistance versus temperature was used to determine the TCR (without normalization).

The crystallite size of ruthenium oxide under different processing conditions was estimated from X-ray diffraction data based on the full-width-at-half-maximum (FWHM) of the RuO_2 (110) peak. The crystallite size estimates determined by X-ray diffraction were qualitatively consistent with transmission electron microscopy (TEM) observation. Details of these measurements and observations have been reported in the previous paper.[2]

RESULTS AND DISCUSSION

The typical processing conditions for the resistor ink and LTCC tape are 850 °C for 20 minutes, as suggested by the vendor. Our measurements indicated that the sheet resistance values did not show a high degree of variation under typical processing conditions, and for the most part the material behaved within the manufactures

specifications. The selection of peak temperatures and time ranges in this study extends beyond the manufactured specifications. Extending these processing temperature/time ranges was necessary to obtain the trends that were needed to specifically understand these materials and their microstructure changes from a mechanistic viewpoint. Furthermore, for high frequency applications, a higher firing temperature or a longer soaking time is sometimes desirable. From a performance perspective, further densification of the conductor material can help minimize high frequency impedance loss of the conductor traces. The results of this systematic study can also serve to determine the extent of valid firing ranges as well as what behaviors can be expected for samples processed outside of the standard processing space.

(I) Microstructure Development

During the sintering process, the glass in the resistor underwent a tremendous change. Glass particles first melted and wet the RuO_2 particles, then the large glass particles devitrified, and after a long sintering time a significant Ostwald ripening of RuO_2 grains occurred. X-ray data indicated that during these thermal events, the nano-size ruthenium oxide particles gradually increased their crystalline size from an average size from 300Å to 520Å. Fig. 3 shows the crystallite size changes with processing time for a sample processed at 875 °C. Data showed that the particles grew at a relative fast rate at the beginning of the process then slowly leveled off after 3 hours. Presumably all the extremely fine RuO_2 crystallites initially in the paste have been completely consumed during the early stages of the ripening process. This postulate is supported by the direct Transmission Electron Microscopy (TEM) observation of our buried resistors.[2] The minimum particle size showed a dramatic increase when the processing temperature and time was increased from 835 °C for 10 minutes to 875 °C for 60 or 720 minutes. Similar observations were reported for a post-fired ruthenate-based resistor, where the finest particles seem to disappear in a much faster rate within a short period of time (10 minutes at 850°C).[8] These observations suggest that as the sintering time gets longer, larger grains continue to grow at the expense of smaller particles. This is a classic example of Ostwald ripening.[9] Since the total amount of ruthenium oxide in the resistor is pre-determined by the ink formulation, ripening will lead to an increase in the particle-particle separation between conductive oxide particles. This is especially true when

extended ripening occurs (exaggerated grain growth). In spite of the involvement of a devitrication process, ruthenium oxide particles in buried resistors were observed in the residual glass phase between a random array of large devitrified glass particles.[2] Therefore, the overall picture of charge carriers tunneling through thin glass barriers along the three-dimensional network of conductive particle chains remains unchanged.

(2) Modification of the Tunneling Barrier Model

From the previous section, we found that ripening brings two major changes to the resistor microstructure, namely the coarsening of ruthenium oxide particles and the increase in particle-particle separation. The original model discusses some particle size effects on the resistance of thick film resistors.[4] However, the effect of changing the particle-particle separation in the resistor was not included, presumably due to the scope of their work. It is well know that the tunneling probability falls off exponentially with barrier thickness. Barrier layers thicker than a few tens of angstroms are nearly impenetrable to tunneling electrons under low field. Although this physical picture properly describes the drop of the tunneling probability, the actual estimation of the particle-particle separation that can statistically represent a complex three dimensional particle chain structure is a formidable task. Since the electrical properties are sensitive to slight changes in particle-particle separation, in this work we have added an additional factor, $D(E, s)$, into the lump term R_{bo} to acount for the tunneling probability of a charge carrier with charging energy E as a function of particle-particle separation s. Finally, we combine $R_{bo}/D(E, s)$ into a new term, R_{bo}'. Therefore, the original expression can be written as

$$R(T) = \frac{1}{2}\frac{R_{bo}}{D(E,s)}\left(\frac{\sin aT}{aT}\right)\left[1+\exp\left(\frac{E}{kT}\right)\right] + R_{mo}(1+bT),$$

$$\therefore R(T) = \frac{1}{2}R_{bo}'\left(\frac{\sin aT}{aT}\right)\left[1+\exp\left(\frac{E}{kT}\right)\right] + R_{mo}(1+bT). \qquad (2)$$

Now, R_{bo}' represents the electrical property changes associated with particle-particle separation. For example, when the value of R_{bo}' becomes greater, it suggests that the tunneling probability in the resistors might have decreased due to the increase in the particle-particle separation. Although we present no quantitative measurement of $D(E, s)$ and the general appearance of the original equation has not changed, the modified form

provides a qualitative interpretation about how processing conditions affect the microstructure, and in turn, electrical properties of the resistors.

Because the charging energy E is typically small (on the order of 1000μeV), the $\exp(E/kT)$ term can be approximated by $(1+E/kT)$. In addition, the values of a for our problem are also expected to be ~(5-10) X 10^{-4} K^{-1}; therefore, the product aT is <<1.[10,11] With these assumptions and modifications, the approximate R(T) from Eq. (2) can be expressed as

$$R(T)=\frac{1}{2}R_{bo}\left(1-\frac{a^2T^2}{6}\right)\left(2+\frac{E}{kT}\right)+R_{mo}(1+bT) \qquad (3)$$

Preliminary curve fitting (based on Eq. (3)) confirmed that values for a are relatively small, ranging from (1.63 – 1.98) X 10^{-4} K^{-1}; therefore, the overall weak temperature dependence of the tunneling effect described by the $(1-a^2T^2/6)$ term is close to unity. Consequently, Eq (3) can be further simplified as

$$R(T)=\frac{1}{2}R_{bo}\left(2+\frac{E}{kT}\right)+R_{mo}(1+bT) \qquad (4),$$

where b can be assumed to be a constant value of 520 ppm/°C, based on conclusions from the original model.[4] In this study, all the final data analyses of $R(T)$ in these cases were performed using Eq (4). This simplification made in Eq (3) and Eq. (4) reduces the relative dependence of multi-parameters in the curve fitting routine and highlights the important factors that can be correlated to microstructure changes. Based on the experimental data and physical meanings of these terms involved, two initial constraints were placed for the curve fitting routine. First, R is greater than the resistance value at room temperature and second, the charging energy is greater than zero. The results of these model parameters determined by the curve fitting have been tabulated in Table 1. Based on the correlation factor, r^2 (see Table 1), the quality of the curve fitting for samples measured in this investigation is excellent.

Eq. (4) shows that $R(T)$ also depends on the magnitude of the charging energy E. In fact, the microstructure change associated with the ripening process has a profound effect on charging energy. By treating the tunneling phenomenon as the movement of charge carriers between two electrodes strictly due to electrostatic effects, the effective capacitance C between particles will scale with the particle size. Smaller particles with

finite electrode size possess smaller effective capacitance between particles. As a result, the energy required to transfer a charge from one particle to the other will be greater ($E = Q^2/2C$). Previous work[4,12] has indicated that the charging energy should exhibit an inverse proportional relationship with the particle size. By the same token, as the particle-particle separation between conducting particles increases the effective capacitance C decreases and results in a greater E. Since the second term in Eq. (4) is derived from the Fermi function, the increase in charging energy implies a decrease in the total number of charge carriers that are readily available for tunneling. As a result, resistors with a higher charging energy will have a greater resistance. These microstructure effects on E and R_{bo}' will be discussed in more detail together with resistance and TCR results.

(3) The Electrical Resistance

Figure 4 shows the effect of firing temperature and processing time (t) on the sheet resistance of buried resistors in the low temperature co-fired ceramic. In general, over this time range the sheet resistance decreases as the sintering time increases. In addition, the peak sintering temperature exhibits a more prominent effect; the sheet resistance drops almost 40% from 825°C to 875 °C. This effect is shown in Figure 5 where samples were sintered for 40 minutes at their respective peak temperatures. These results suggest that when processing samples at higher temperatures, precise control of the process time is an important parameter for reproduciblility.

When samples were held at 875 °C for longer than an hour the resistance values reached a minimum value and started to increase again (see Figure 6). Data also indicate that the time required to reach the resistance minimum is strongly dependent on the peak firing temperature. For example, it took an additional 60 minutes to reach the minimum sheet resistance for samples prepared at 850 °C in comparison with samples prepared at 875 °C (Figure 6). These results suggest that a kinetic factor dependent on the processing temperature is involved in the changes in the electrical properties. The kinetic factor could be due to chemical reactions or microstructural changes in the resistor during processing. In spite of three different crystalline phases developed from the glass, both X-ray and TEM results show that RuO_2 is stable in the buried resistors.[2] Although it is difficult to rule out the effect of a slight chemical modification in glass on tunneling

behavior, it has been reported that the transport properties of RuO_2 based resistors in the vitreous glass systems appear to be rather independent of the gross composition of the glass.[3,4] Furthermore, the electrical properties of the resistors buried in LTCC packages compared to those printed on alumina substrates show no significant difference (see Fig. 2). This suggests that the kinetics involving possible chemical reactions between the dielectric layer and resistor do not play an important role in determining the final electrical properties. Therefore, in this investigation we focus on the kinetic issues related to the microstructure development in the resistor under different processing conditions. Special attention is paid to samples prepared at 875 °C where all the kinetics are faster.

For the convenience of discussion, a schematic of microstructural development during the ripening process is illustrated in Fig. 8, based on our TEM observations.[2] In this figure, the small gray circles represent the extremely fine oxide particles that are present in the initial resistor ink, the medium size open circles represent medium size conducting particles, and the large solid circles are for the large RuO_2 particles in the resistor. During the initial ripening process, some extremely fine particles are rapidly consumed and additional medium size particles are created. This is represented by a progressive change in microstructure from the initial sintering process (a) to the lowest resistance point (b) where the medium size particle is dominant in the microstructure. As ripening continues, the finest particles will completely disappear and some medium particles are consumed. Eventually, exaggerated grain crystal growth occurs (as illustrated by one largest solid circle in Fig. 8(c)) and the particle-particle separation increases.

Samples prepared at 850 °C and 875 °C show initial decrease and later increase in resistance suggesting that there might be two different mechanisms that control the conduction behavior before and after the resistance reaches its minimum point. From Eq. (4), it is found that R(T) relies on both R_{bo}' and E which are both dependent on the microstructure in the resistor. R_{bo}' depends on particle-particle separation and E depends on particle size. Results from Table 1 show that both *Rbo*' and E first decrease then increase as processing time increases. Since the charging energy is inversely proportional to the crystalline size, the initial decrease in E ($t < 60$ min.) can be readily

explained in terms of coarsening of ruthenium oxide particles as observed in Fig. 3. However, when extended ripening occurs and particle-particle separation s increases (see the changes between Fig. 8(b) and Fig. 8(c)), the effective capacitance between particles decreases. As a result, the charging energy rises again (t >60 min.).

The drop in R_{bo}' as a function of processing time during the initial stage ($t < 60$ min.) is a more complex issue. As discussed earlier, fine particles have a smaller cross-sectional area for tunneling[13] and a high charging energy which reduces the number of charge carriers capable of tunneling. Smaller particles, therefore, are relatively "inactive" and will not contribute much to the overall electrical conduction. Under a weak field, the charge carriers traveling through the resistor tend to utilize the low-charging energy, low resistance chain segments in the three-dimensional conductive paths. As a result, the overall conductance is determined by the tunneling between those relatively large particles. Such an effect is more important at the beginning of the sintering process when there are more extremely-fine conductive particles in the resistor. Therefore, within this period ($t < 60$ min.) a longer processing time not only increases the average crystalline size but more importantly aids in the building of more effective conducting paths. The later process, in fact, reduces the effective particle-particle separation (as illustrated in Fig 8(b) where more conducting paths are available along the medium size circles) and results in the decrease in R_{bo}'. As processing time extends beyond the period (t > 60 min.), more and more particles disappear and the increase in particle-particle separation (see Fig. 8(c)) reduces the tunneling probability $D(E,s)$, and R_{bo}' starts to rise again.

Because the charging energy decreases with particle size and increases with particle-particle separation, the fact that the charging energy reduces to a minimum at 60 minutes suggests that an optimum microstructure in the resistor ink has developed. At this point, the ripening process has provided more "active" conducting particles for the conduction while the tunneling probability has not yet been deteriorated by the increase in particle-particle separation. As a result, both resistance and R_{bo}' reach their minimum value.

Since ripening of the conductive ruthenium oxide particles is determined by the kinetics of mass transport in the glass matrix, both processing temperature and firing time will have a strong effect on the final microstructure. In general, the kinetics of mass

transport is exponentially proportional to the processing temperature. Therefore, when samples are fired at higher temperature, the time for the resistance value to reach a minimum becomes shorter as shown by the experimental results in Fig. 6.

(4) Temperature Coefficient of Resistance

TCR is a measurement of the slope of the resistance versus temperature. Industry convention characterizes the TCR based on the following equation

$$\text{TCR (ppm/°C)} = \frac{(R(T_2) - R(T_1))}{(T_2 - T_1) * R(T_1)} * 10^6. \quad (5)$$

Typical changes in TCR for standard thick film resistors are within 100 ppm/°C.[8] Because of the characteristics of the R(T) curve, the TCR has been further divided into hot and cold TCR values corresponding to the positive and negative slope sections of R(T) curve. Since the scope of this investigation is to understand the physical issues underlying the property changes, the reported TCR values in this paper were not normalized by the reference resistance value R(T_1).

The change of resistance as a function of temperature for buried resistors processed at 875 °C for different times is given in Figure 8. The TCR (not normalized, ohm/°C) for these resistors was determined by a least square method. It was found that when these values were normalized with respect to a resistance value at 0 °C (Eq. (5)) the normalized TCR values range from 114 to 312 ppm/°C, which are greater than the traditional post-fired resistors (<100 ppm/°C).[6] Results also show that the TCR of these buried resistors are all negative, indicating that the conductance of the metal oxide component from Eq. (4) is insignificant within the temperature range we have studied (-100°C to 100°C), as demonstrated from the relatively small values of R_{mo}.in Table 1 (in the order of 10^{-8} to 10^{-9} ohms). Therefore, the limiting conduction mechanism in these buried resistors is determined by the tunneling barrier of the glass phase between oxide particles. Similar behaviors were observed from samples fired at 835 and 850 °C for forty minutes, and the values of TCR for these samples are summarized in Table 1. The relatively high value of TCR (normalized) and negative slope of R(T) of these buried resistors have also been observed by Rellick and Ritter.[14] Coincidentally, the TCR of these resistors follows the same trend as the sheet resistance, where the absolute TCR

value reaches a minimum at 60 minutes then increases again as processing time increases (see Table 1).

From the first derivative of Eq. (4), it can be shown that TCR of these resistors is linearly dependent on the charging energy. This effect is directly illustrated in Fig. (9), where charging energy is plotted against TCR. Although these samples were prepared under different conditions, the results show a good correlation between TCR and charging energy. Since charging energy varies with the ripening of ruthenium oxide particles in the resistor, from a processing perspective both charging energy and TCR should follow the same trend as the resistance when processing time elapses. The trade-off between particle growth and particle-particle separation should lead a minimum for E and TCR. As a result, both E and TCR reach their minimum value at 60 minutes. The time that both resistance and TCR reach their minimum point, therefore, is not a coincidence.

The physical connection between charging energy and TCR can be explained in terms of changes in the re-distribution of the carrier population by temperature. Using the Fermi function[15], the relative changes in the temperature dependence of probability for a charge carrier occupying a higher charge state are greater than that of one at a lower state. As the temperature changes, resistors with a higher charging energy will experience a large fluctuation in the number of charge carriers that are capable of tunneling. The greater fluctuation in the number of charge carriers with respect to temperature leads to a higher TCR. As a result, samples prepared for a shorter sintering time or those that experienced extended ripening will have greater TCR values.

The microstructure developed at the resistance minimum, therefore, represents an optimum microstructure. Resistors processed at this optimum condition are highly desirable since the variation of resistance is less sensitive to the processing time and TCR achieves a minimum value. This combination leads to a robust process that will provide resistors with high tolerance and excellent temperature performance.

CONCLUSION

The conduction mechanism for buried resistors in this study is predominantly determined by tunneling between ruthenium oxide particles. The electrical properties of the resistor do not appear to be strongly affected by the changes in bulk composition of the glass or by the complicated devitrification process that occurs during sintering. Results suggest that the electrical properties, processing, and resulting microstructures are closely related. The original tunneling barrier model was slightly modified to more accurately account for the changes in microstructure as ripening of the conductive oxide occurs. Model parameters determined from curve fitting indicated that an optimum microstructure exists where the charging energy reaches a minimum and the tunneling probability is at a maximum. When this optimum microstructure is approached, the resistance value will be less sensitive to the variations in the processing time and the TCR will achieve a minimum absolute value. These results provide a physical interpretation to the effect of processing conditions on the electrical properties and give a guideline for processing buried resistors to achieve high tolerance and excellent temperature performance.

ACKNOWLEGEMENT

The authors acknowledge many insightful discussions with Gordon. E. Pike and Carleton H. Seager, and would also like to thank Motorola for providing the experimental resistor ink for this investigation. Sandia is a multiprogram Laboratory operated by Sandia Corporation, a Lockheed Martin Company, for the United States Department of Energy under Contract DE-AC04-94AL85000.

REFERENCES

1. M. A. Rodriguez, P. Yang, P. Kotula, and D. Dimos, "X-ray Characterization of Resistor/Dielectric Material for Low Temperature Co-Fired Ceramic," to be published in *Adv. X-ray Anal.*, **43**, (1999).
2. M. A. Rodriguez, P. Yang, P. Kotula, and D. Dimos, "Microstructural and Phase Development for Buried Resistors in Low Temperature Co-Fired Ceramic," to be submitted to *J. Am. Ceram. Soc.*, (1999). (to be determined –Electroceramics?)
3. R. W. Vest, "A Model for Sheet Resistivity of RuO_2 Thick Film Resistors," *IEEE Trans. Compon. Hybrids, and Manufact. Technol.*, **14** [2] 397-406 (1991).
4. G. E. Pike and C. H. Seager, "Electrical Properties and Conduction Mechanisms of Ru-based Thick-Film (Cermet) Resistors,"*J. Appl. Phys.*, **48** [12] 5152-5169 (1977).
5. R. Stratton, "Volt-Current Characteristics for Tunneling Through Insulating Films," *J. Phys. Chem. Solids.*, **23** 1177-1190 (1962).
6. P. Yang, unpublished data.
7. P. Yang, D. Dimos, M. A. Rodriguez, R. F. Huang, S. Dai and D.Wilcox, "Direct-Write Precision Resistors for Ceramic Packages,"; pp. 159-164 in Materials Research Society. Symposium Proceedings. Vol. 542, Ceramic Freeform and Layered Direct Fabrication, Materials Research Society, Pittsburgh, PA, 1999.
8. F. Johnson, G. M. Crosbie, W. T. Donlon, "The Effects of Processing Conditions on the Resistivity and Microstructure of Ruthenate-Based Thick Film Resistors," *J. Mat. Sci.- Materials in Electronics.*, **8** 29-37 (1997).
9. W. D. Kingery, H. K. Bowen and D. R. Uhlmann, 2nd Edition, Chapter 9, John Wiley & Sons, Inc. New York, NY 1976.
10. G. M. Crosbie, F. Johnson and W. Trela, "Processing Factor Dependence of Resistivity Parameters of Ruthenate-Based Thick Film Resistors with Low Temperature Coefficients," *J. Appl. Phys.*, **84** [5] 2913-2919 (1998).
11. G. E. Pike and C. H. Seager, Sandia Technical Report, SAND76-0558 (1977).
12. W. R. Smyth, Static and Dynamic Electricity, McGraw_Hill, New York, NY 1968; An example for the microstructure effects on the electrical properties of a post-fired resistor is given by B. Morten, A. Masoero, M. Prudenziati and T. Manfredini, "Evolution of Ruthenate-Based Thick Film Cermet Resistor," *J. Phys. D: Appl. Phys.*, **27** 2227-2235 (1994).
13. G. E. Pike, private communication.
14. J. R. Rellick and A. P. Ritter, "Non-Trimmed Buried Resistors in Green Tape Circuits," *Int. Conf. On High Density Packag. & MCMs.*,1-5 (1999).
15. C. Kittel, Introduction to Solid State Physics, 5th Edition, Chapter 6, John Wiley & Sons, Inc. New York, NY 1976.

Captions

Fig.1. Temperature dependence of resistance of a post-fired ruthenium oxide based thick film resistor.

Figure 2. Resistance of buried (open circles) and post-fired (solid circles) resistors as a function of dry film thickness. Samples were fabricated from the the same buried resistor ink and were fired at 875 °C for 20 minutes.

Figure 3. Average particle size versus processing time for buried resistors fired at 875 °C.

Figure 4. Sheet resistance of buried resistors fired under different processing conditions

Figure 5. Sheet resistance as a function of peak firing temperature. Samples were held at the peak temperature for 40 minutes.

Figure 6. The variation of sheet resistance as a function of processing time and firing temperature.

Figure 7. A schematic illustration of the microstructural changes associated with the Ostwald ripening (a) initial sintering stage ($t < 60$ min.), (b) optimum microstructure ($t =$ 60 min.) and (c) extended ripening ($t > 60$ min.). (see details in the text).

Figure 8. Temperature dependence of resistance for buried resistors processed at various times. The open circles are the experimental data and solid lines are calculated based on Eq. (4)

Figure 9. Temperature coefficient of resistance versus charging energy.

Table I. Processing conditions, TCR, and model parameters determined by curve fitting routine.

Processing Conditions	TCR (ohms/°C)	R_{bo}' (ohms)	E (μeV)	R_{mo} (ohms)	r^2
835 °C, 40 min.	-0.1354	711.2	1848	35.72×10^{-9}	0.946
850 °C, 40 min.	-0.1000	650.2	1737	37.17×10^{-9}	0.924
875°C, 5 min.	-0.1406	734.7	2352	19.91×10^{-9}	0.996
875°C, 20 min.	-0.0725	527.0	1697	8.86×10^{-9}	0.987
875°C, 60 min.	-0.0542	459.1	1435	6.85×10^{-9}	0.989
875°C, 240 min.	-0.3089	914.1	4148	45.57×10^{-9}	0.977
875°C, 720 min.	-0.3386	998.7	3756	9.01×10^{-9}	0.968

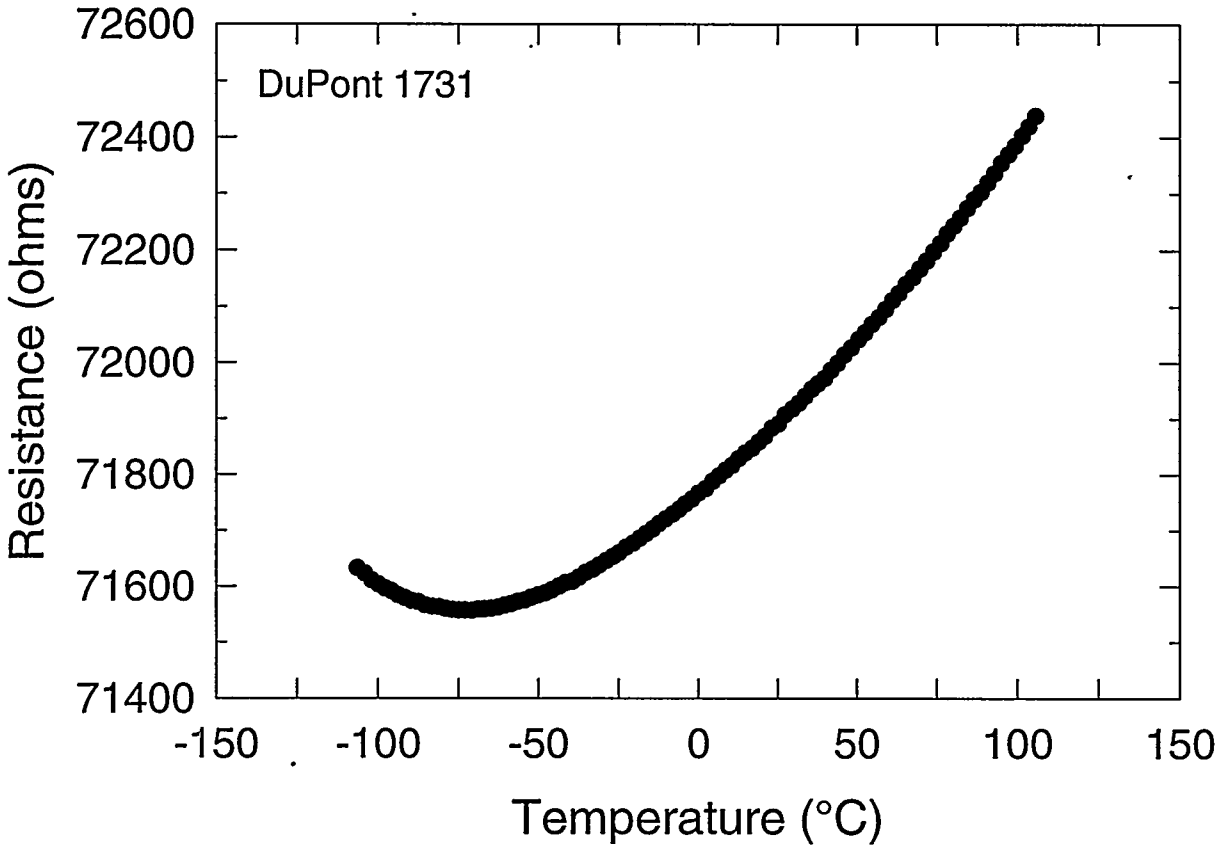
DuPont 1731
Resistance (ohms)
72600
72400
72200
72000
71800
71600
71400
-150
-100
-50
0
50
100
150
Temperature (°C)

Fig. 1

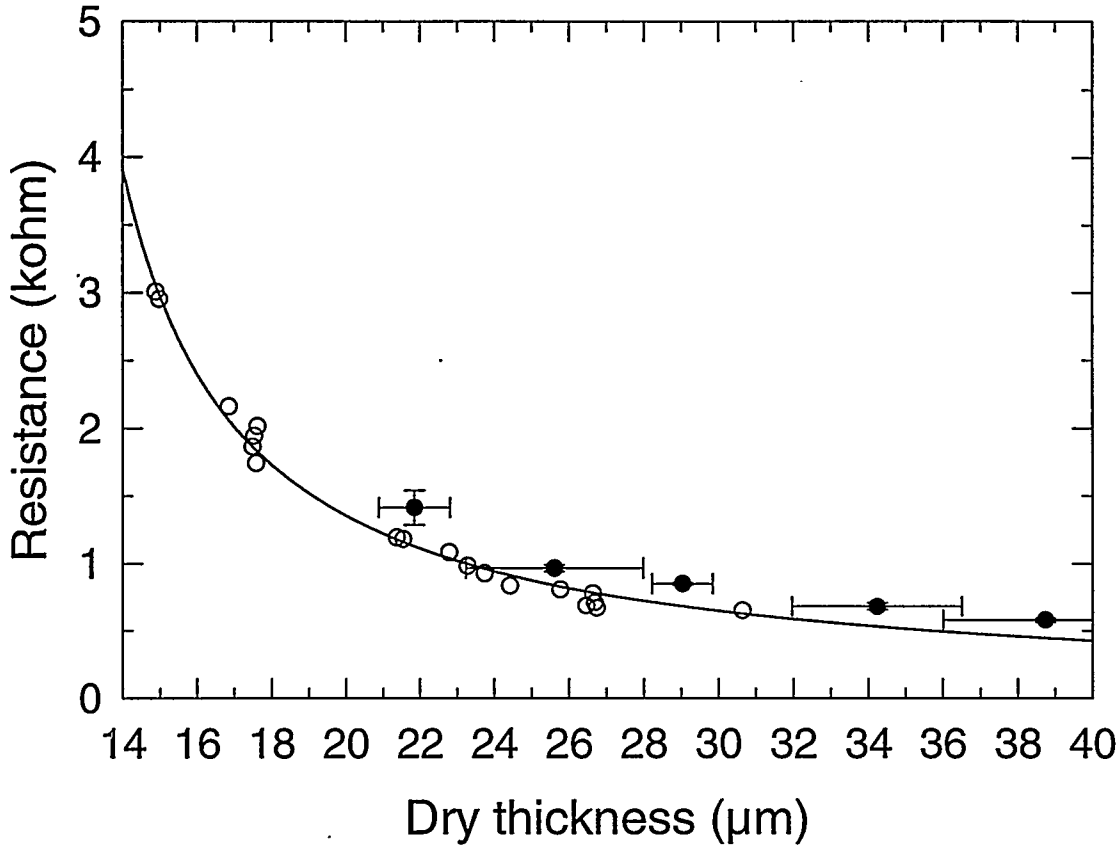
Resistance (kohm)
0
1
2
3
4
5
14
16
18
20
22
24
26
28
30
32
34
36
38
40
Dry thickness (µm)

Fig. 2

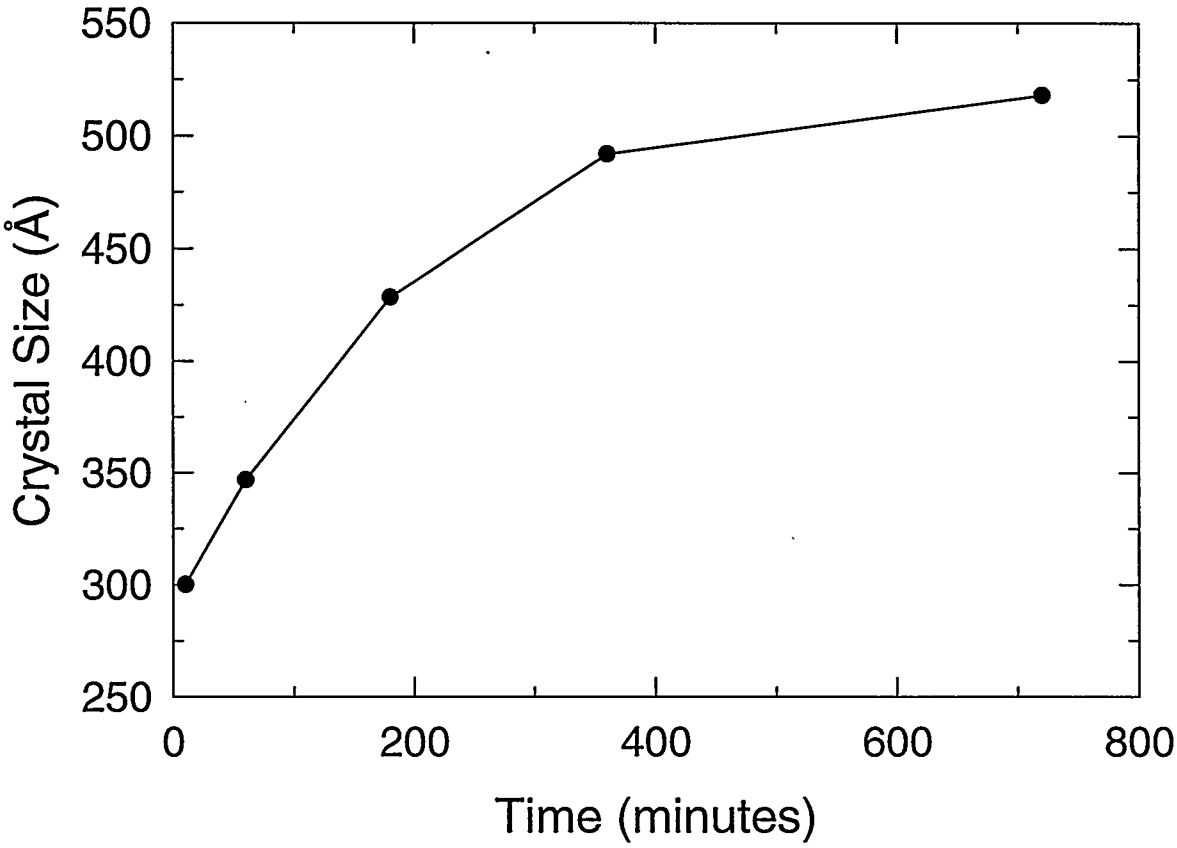
550
500
450
400
350
300
250
Crystal Size (Å)
0
200
400
600
800
Time (minutes)

Fig. 3

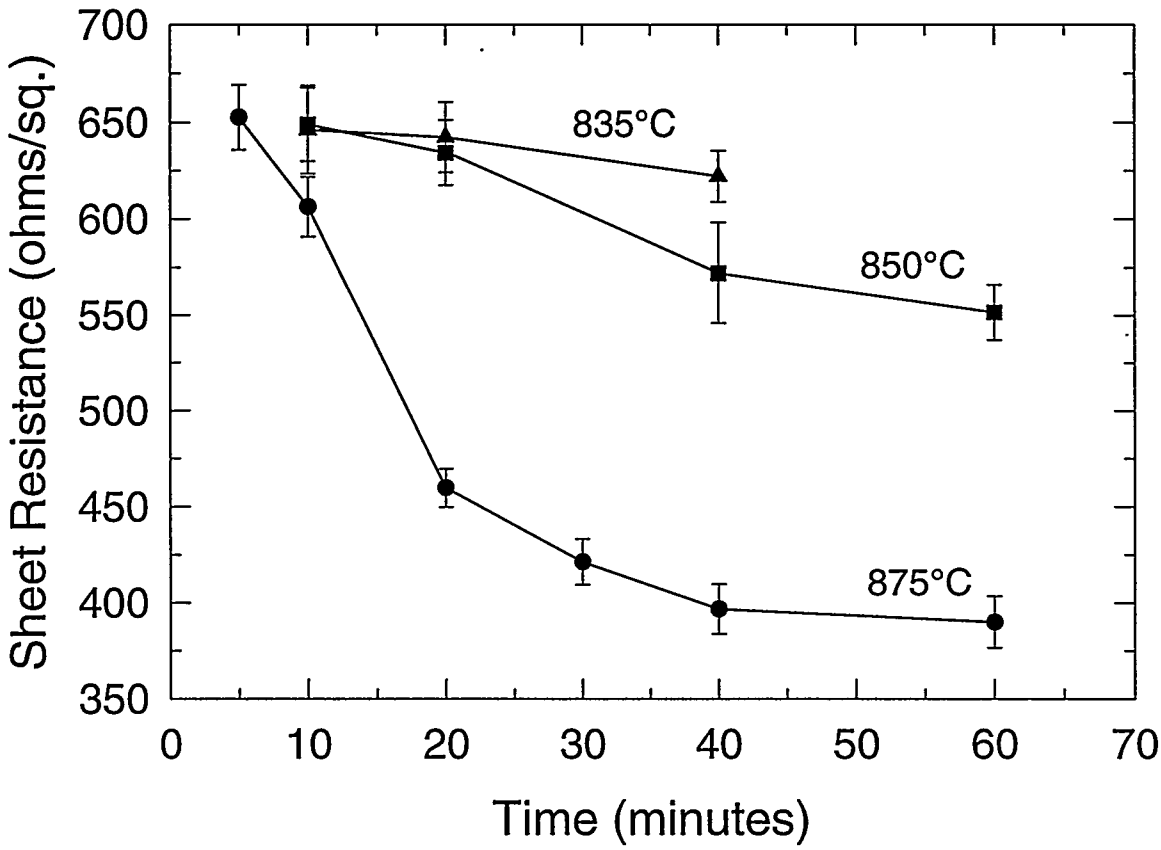
Sheet Resistance (ohms/sq.)
700
650
600
550
500
450
400
350
0
10
20
30
40
50
60
70
Time (minutes)
835°C
850°C
875°C

Fig. 4

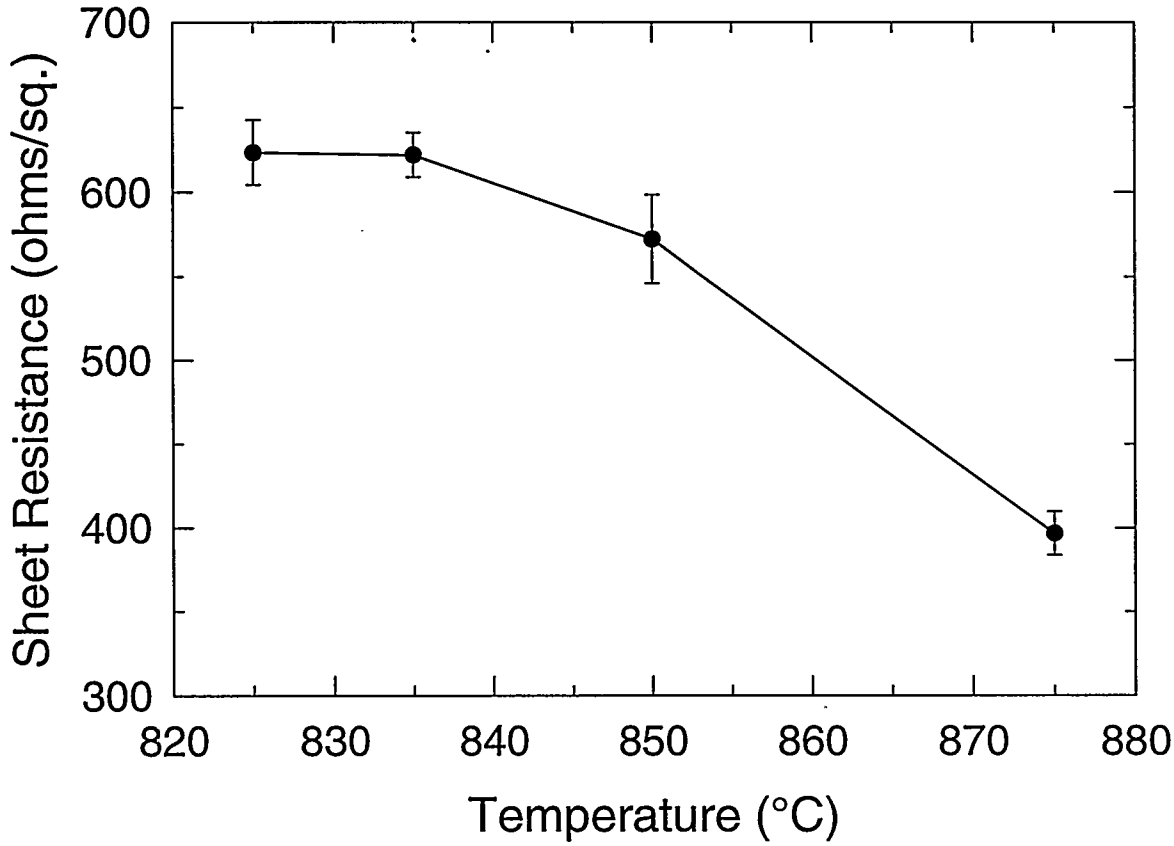
Sheet Resistance (ohms/sq.)
700
600
500
400
300
820
830
840
850
860
870
880
Temperature (°C)

Fig.5

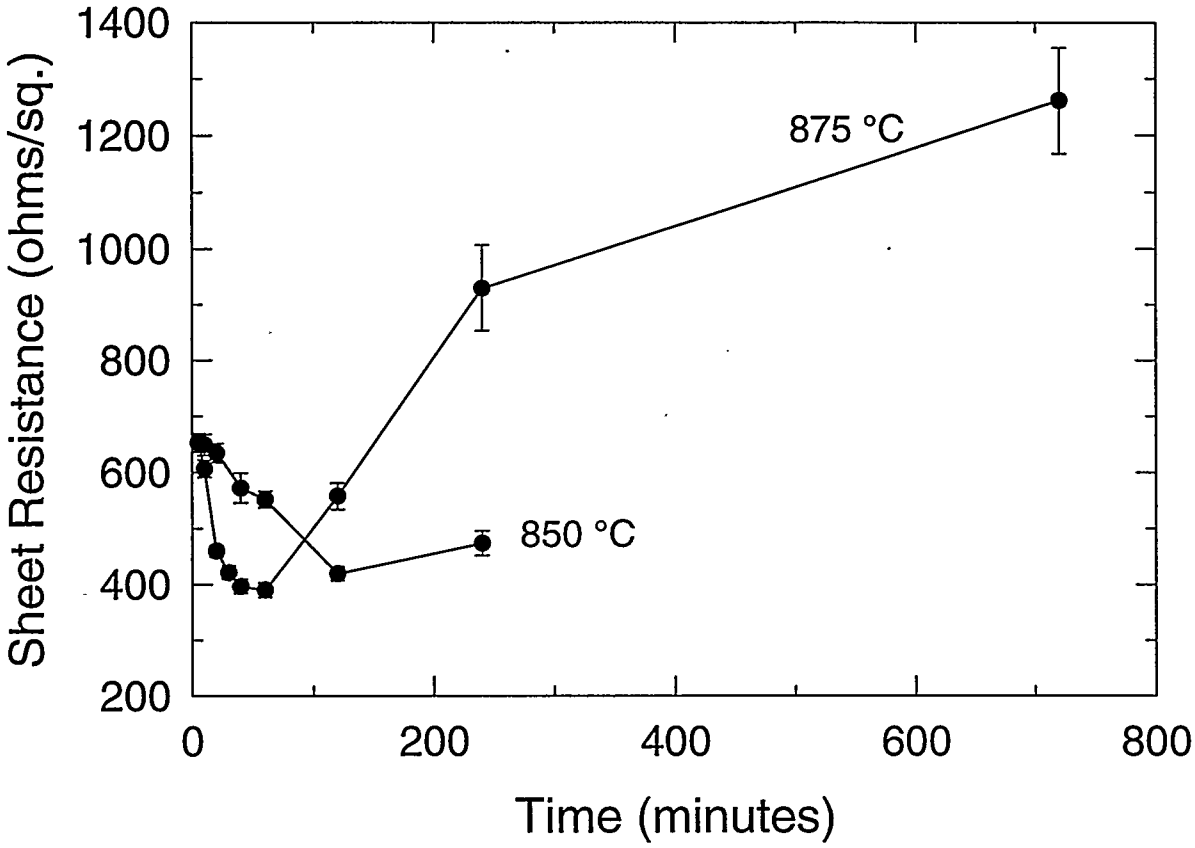
1400
1200
1000
800
600
400
200
Sheet Resistance (ohms/sq.)
0
200
400
600
800
Time (minutes)
875 °C
850 °C

Fig. 6

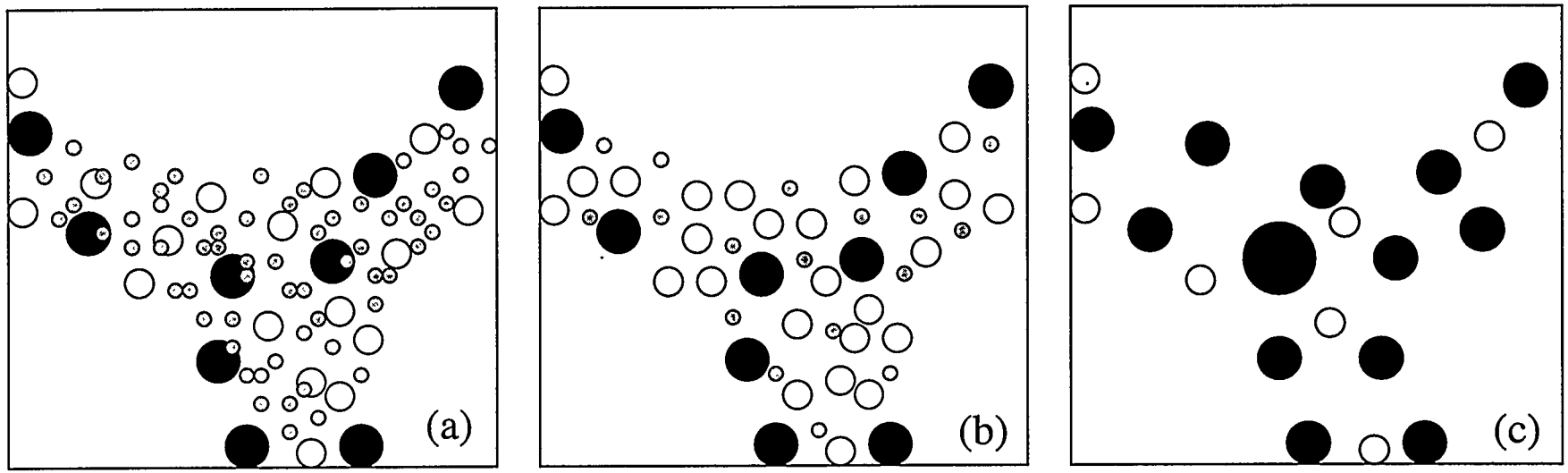

Fig. 7

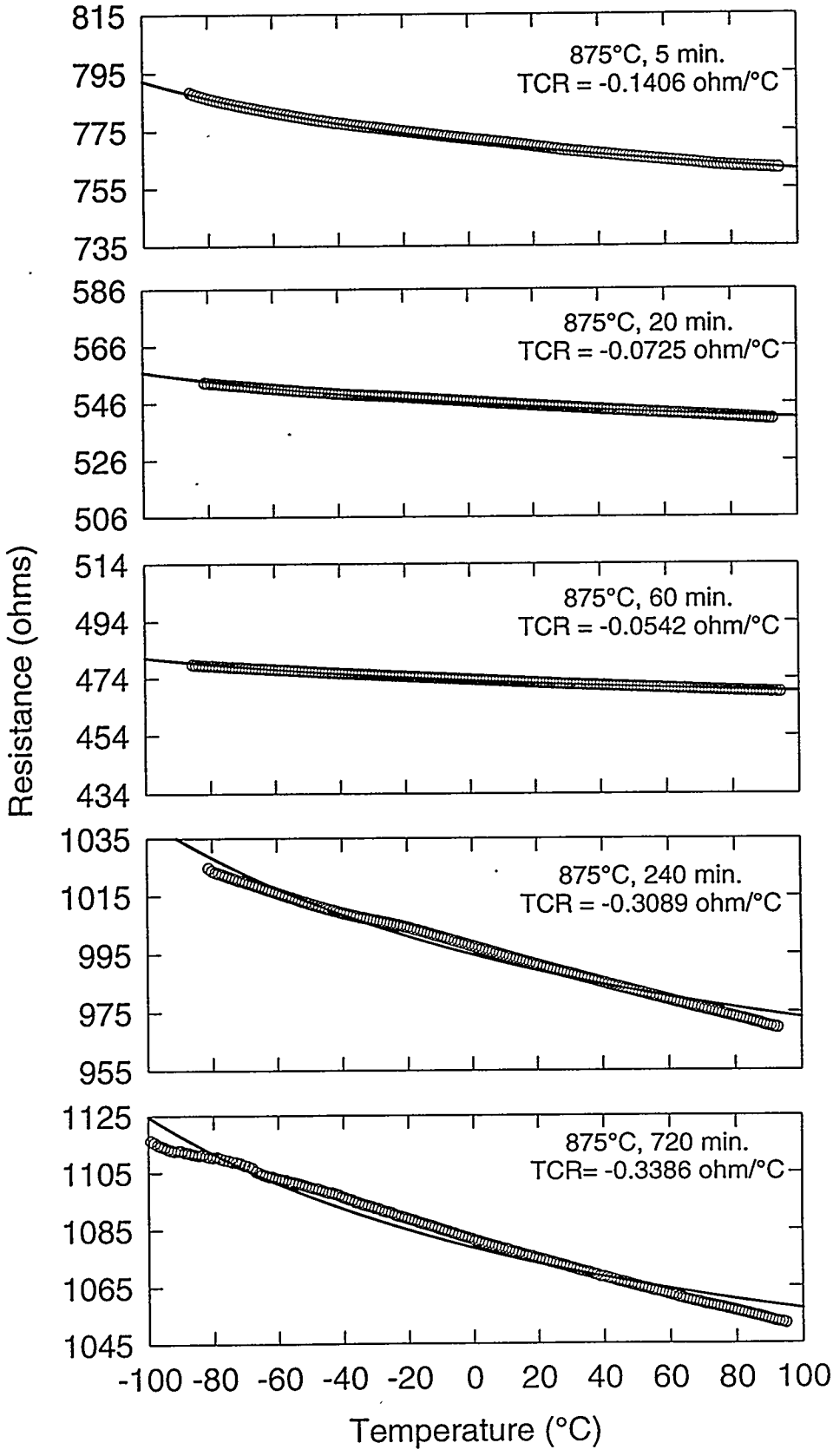
875°C, 5 min.
TCR = -0.1406 ohm/°C
875°C, 20 min.
TCR = -0.0725 ohm/°C
875°C, 60 min.
TCR = -0.0542 ohm/°C
875°C, 240 min.
TCR = -0.3089 ohm/°C
875°C, 720 min.
TCR= -0.3386 ohm/°C
Resistance (ohms)
815
795
775
755
735
586
566
546
526
506
514
494
474
454
434
1035
1015
995
975
955
1125
1105
1085
1065
1045
-100 -80 -60 -40 -20 0 20 40 60 80 100
Temperature (°C)

Fig 8

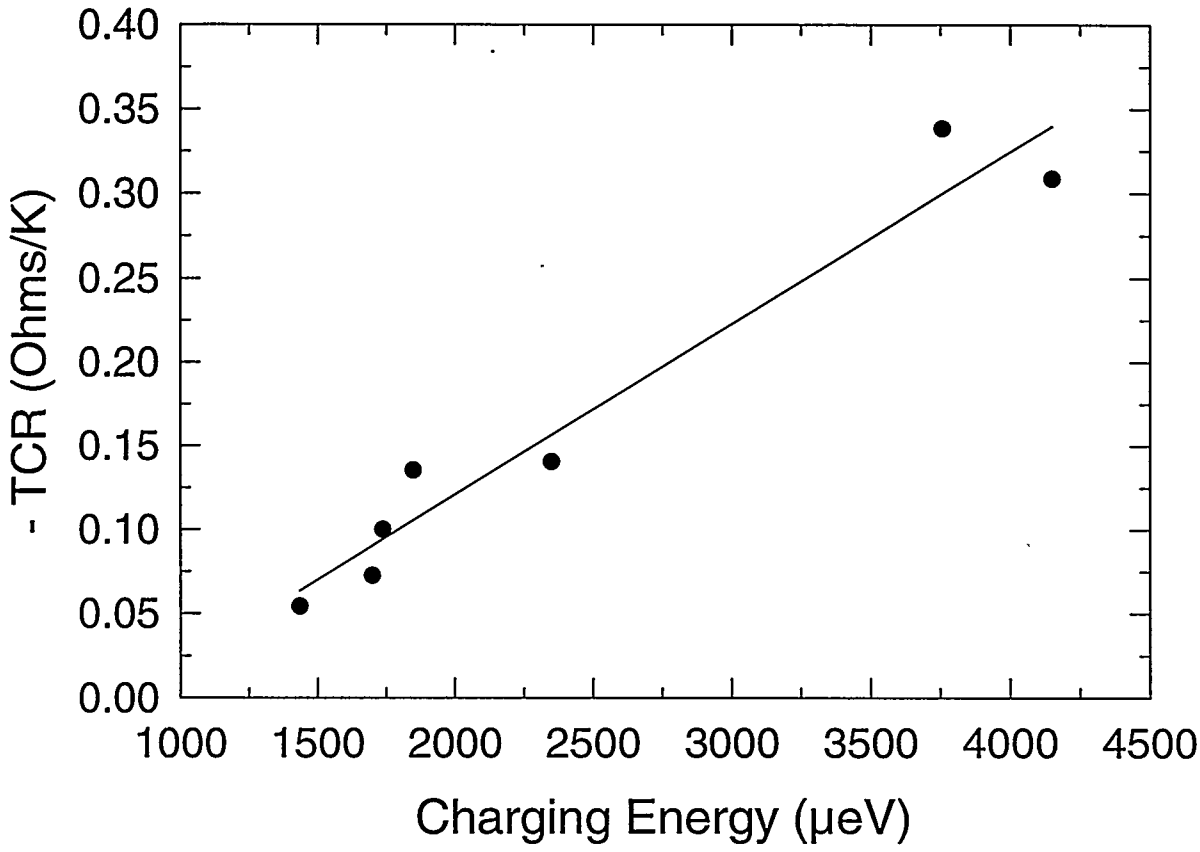
0.40
0.35
0.30
0.25
0.20
0.15
0.10
0.05
0.00
- TCR (Ohms/K)
1000
1500
2000
2500
3000
3500
4000
4500
Charging Energy (μeV)

Fig. 9